metals

MDPI

Article

Assessment the Partial Welding Influences on Fatigue Life of S700MC Steel Fillet Welds

Jaromir Moravec *, Jiri Sobotka, Iva Novakova and Sarka Bukovska

Department of Engineering Technology, Faculty of Mechanical Engineering, Technical University of Liberec, Studentská 1402/2, 46117 Liberec, Czech Republic; jiri.sobotka@tul.cz (J.S.); iva.novakova@tul.cz (I.N.); sarka.bukovska@tul.cz (S.B.)

* Correspondence: jaromir.moravec@tul.cz; Tel.: +420-485-353-341

Abstract: Fine-grained steels belonging to the HSLA group (High-Strength Low-Alloy steels) of steels are becoming increasingly popular and are used in both statically and dynamically stressed structures. Due to the method of their production, and thus also the method use to obtain the required mechanical properties, it is really necessary to limit the heat input values for these steels during welding. When applying temperature cycles, HSLA steels in highly heated heat-affected zones (HAZ) reveal intensive grain coarsening and also softening behaviour. This subsequently results in changes in both mechanical and brittle-fracture properties, and the fatigue life of welded joints. While grain coarsening and structure softening have a major effect on the change of strength properties and KCV (Charpy V-notch impact toughness) values of statically stressed welded joints, the effect of these changes on the fatigue life of cyclically stressed welded joints has not yet been quantified. The paper is therefore conceived so as to make it possible to assess and determine the percentage impact of individual aspects of the welding process on changes in their fatigue life. To be more specific, the partial effects of angular deformation, changes that occur in the HAZ of weld, and the notch effect due to weld geometry are assessed.

Keywords: HSLA steels; fatigue life of welds; heat affected zone; notch effect; angular deformation; S-N curves

check for updates

Citation: Moravec, J.; Sobotka, J.; Novakova, I.; Bukovska, S. Assessment the Partial Welding Influences on Fatigue Life of S700MC Steel Fillet Welds. *Metals* **2021**, *11*, 334. https://doi.org/10.3390/met11020334

Academic Editor: Joseba Albizuri

Received: 22 January 2021

Accepted: 12 February 2021

Published: 16 February 2021

Publisher's Note: MDPI stays neutral with regard to jurisdictional claims in published maps and institutional affiliations.

Copyright: © 2021 by the authors. Licensee MDPI, Basel, Switzerland. This article is an open access article distributed under the terms and conditions of the Creative Commons Attribution (CC BY) license (https://creativecommons.org/licenses/by/4.0/).

1. Introduction

HSLA (High-Strength Low-Alloy) steels are currently one of the preferred types of material among structural steels. Their main advantages include high strength properties, sufficient ductility and very good resistance to brittle failure [1,2], even at sub-zero temperatures [3,4]. These properties are achieved despite the small number of alloying elements used. In addition, through microalloying and strictly monitored chemical composition of the individual types of steels, very good cold formability and constant technological processability can be achieved.

Thermo-mechanically processed fine-grained steels are generally alloyed with a low content of V, Ti and Nb, creating fine precipitates on the grain boundaries. The resulting carbides, nitrides and carbonitrides of the above elements contribute to matrix strengthening and grain refinement [5,6], and together with deformation strengthening, these represent the main mechanisms for HSLA steels, with yield strengths of up to 700 MPa, in achieving the required strength properties. In the case of thermo-mechanically processed steels with a higher yield strength, other strengthening mechanisms (such as, e.g., austenite-to-martensite and bainite phase transformation) are used [7–11].

Due to the low carbon content and a very small number of alloying elements, HSLA steels are easily weldable. However, there are some specifics. First of all, the heat input value must be limited. Moreover, attention must also be paid to the susceptibility to cold cracking. In general, when welding structural steels, the heat input value should not exceed 15 kJ·cm^{-1}. In addition, in the case of welding high-strength fine-grained steels, it is

recommended that the heat input value be reduced to 10 kJ·cm^{-1}, due to both the intensive grain coarsening in the highly heated HAZ and also the softening of the structure that can occur at the interface between HAZ and base material. The effect of grain coarsening on the change of mechanical properties and the decrease of notch toughness values during welding of S700MC steel has already been studied by, e.g., Górka [12], Moravec et al. [2], and Skowrońska et al. [13], and in the case of high-strength steels by, e.g., Mičian [14], and Njock Bayock et al. [10]. The issue of susceptibility to cold cracking has been discussed by, e.g., Fydrych et al. [15]. Many articles have also dealt with simulations of S700MC steel welding, e.g., Kik at al. [16,17].

A lot of very interesting works have also been published in the field of cyclic loading (fatigue testing) of fine-grained HSLA steels. The effect of the heat input value on the changes in the fatigue life of welded joints of steels with yield strengths lower than 550 MPa was investigated by, e.g., Šebestová et al. [18] and Moravec et al. [19]. The fatigue life of welded joints from steel S700MC and produced using the MAG (Metal Active Gas) method has been studied by Lahtinen et al. [20], and the case of steels with higher yield strength has been studied by, e.g., Lago et al. [21] and Kim et al. [22]. However, all of the above-mentioned authors comprehensively evaluated the effect of welding on fatigue life, by determining the S-N curves (stress–life) of the tested welded joints under the conditions defined by the authors. Thus, from the above works, it is not possible to determine the influence of partial aspects of the welding process. It is, therefore, problematic to assess the effect of, for example, a rigid clamping that reduces the angular deformation of given weldment or intensity of changes that occur in the HAZ. Although there are studies that try to cover just these partial influences, these studies also have their limitations. For example, Schmidova et al. [23] assessed the dynamic fracture toughness of dynamically loaded samples from S700MC steel with the application a temperature cycle. However, it was a cycle with a maximum temperature of 800 °C, and with a significantly slower heating and cooling rate than during a real welding process.

The major aim of the research described in the following sections was to define the influence of individual aspects of the welding process on changes in the fatigue life of welded joints, and thus to show which aspects occurring during welding have a fundamental effect on the durability and which ones are only marginal. Attention was focused on quantification of the influence of angular deformation, changes occurring in the HAZ, and the notch effect caused by the weld geometry. Such information should enable designers and technologists to make more relevant decisions with respect to both welded joint design and the subsequent design of WPS (welding procedure specification).

2. Materials and Methods

Structural steel S700MC (1.8974) is classified as a fine-grained micro-alloyed high-strength steel produced by thermo-mechanical rolling. It is material with a guaranteed minimum yield strength of 700 MPa, good cold formability, low carbon content, and reduced sulphur content. It is micro-alloyed with elements such as Al, Ti, Nb and V. Additionally, it is necessary to ensure that the sum of Nb, V and Ti does not exceed 0.22 wt%. The reason for its good applicability lies in the fact that it can maintain constant technological conditions at cold forming, has good weldability, and there is the possibility to reduce the weight of given parts while retaining the required strength properties. It is used in the field of transportation (e.g., chassis frames of cars and trucks or components of wagons), in the production of mining machines, cranes, partial structural units of bridges, etc. The chemical composition of the tested material (HSLA steel S700MC) is shown in Table 1.

The steel used for the experimental fatigue testing was delivered in the form of 12-mm-thick sheet metal and had a ferritic-bainitic structure (see Figure 1). Chemical composition defined by the standard EN 10149-2, as well as chemical composition, which was determined experimentally using a Q4 Tasman spectrometer (Bruker, Germany), as given in Table 1.

Table 1. Chemical composition of steel S700MC (wt%).

Element	C	Si	Mn	P	S	Al	Nb	V
ČSN EN 10149-2	max. 0.12	max. 0.6	max. 2.2	max. 0.025	max. 0.010	min. 0.015	max. 0.09	max. 0.2
Experiment	0.051	0.197	1.916	0.006	0.006	0.038	0.063	0.072
Element	**Ti**	**Mo**	**B**	**N**	**Ni**	**Cr**	**W**	**-**
ČSN EN 10149-2	max. 0.25	max. 1	max. 0.005	-	-	-	-	-
Experiment	0.056	0.113	0	0.013	0.154	0.036	0.035	-

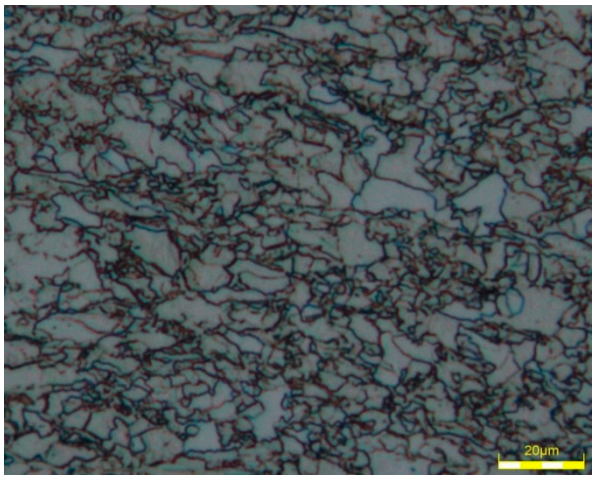


Figure 1. Ferritic-bainitic structure of the tested material—steel S700MC.

A mean grain size of 3.38 µm was determined by EBSD (Electron Back Scatter Diffraction) analysis. This is the average value obtained from three measurements of areas 0.6 mm × 0.6 mm.

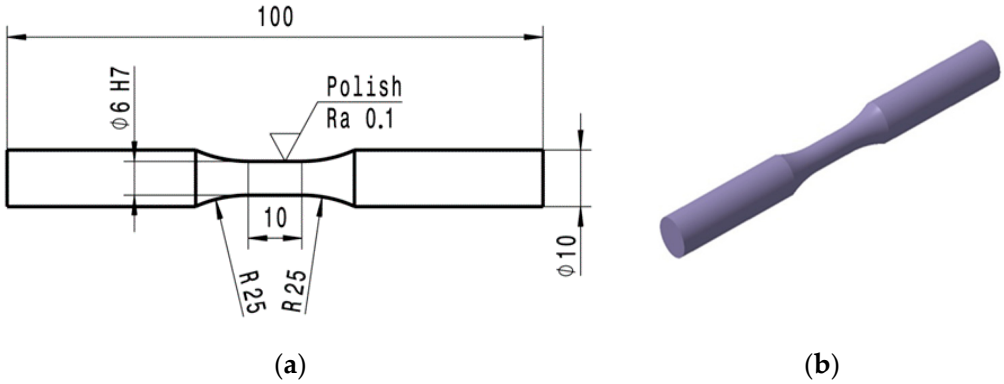
Table 2 shows the basic mechanical properties as determined by the static tensile test. In addition to that, to assess the mechanical properties under dynamic loading, the S-N curve of the base material was also measured. The whole experimental fatigue testing of the base material was performed on the servo-hydraulic device INOVA FU-O-1600-V2 (INOVA GmbH, Bad Schwalbach, Germany), in controlled force mode. For all experiments, only samples with a circular cross-section area were used, in accordance with standard EN 3987—Figure 2.

Table 2. Chemical composition of steel S700MC (wt.%).

Strain Rate (s^{-1})	Sample No.	Diameter of Sample D (mm)	Proof yield Strength $R_{p0.2}$ (MPa)	Ultimate Tensile Strength R_m (MPa)	Uniform Ductility A_g (%)	Total Ductility A_{30} (%)
10^{-2}	BMT-01	6.52	749	851	10.97	23.91
	BMT-02	6.53	748	852	12.33	25.22
	BMT-03	6.50	731	849	10.72	23.62
	BMT-04	6.52	743	853	11.09	23.89
	BMT-05	6.51	739	850	11.14	24.37
	Average Value		**742**	**851**	**11.25**	**24.20**

With respect to the major aim of this paper, experimental measurements were very closely connected with the adjustment of the fatigue testing. For all measurements (1—base material, 2—basic welded samples, 3—welded samples without influence of angular deformation, 4—welded samples without influence of angular deformation and notch effect), test samples were subjected to the given stress amplitudes (levels) under fully reversed harmonic cycle (purely alternating stress) with the stress ratio R = −1 (algebraic ratio of

the minimum stress to the maximum stress). The loading frequency varied depending on the cross-section area of the test samples. In the case of fatigue testing of the base material (S700MC), f = 40 Hz was used. For the rest of the test samples, loading frequency of 20 Hz was used, because of the bigger cross-section area. In addition to this, the loading frequency was also chosen with respect to the possible heating of the sample surface. This is why the infrared pyrometer Mikro-epsilon CTLM-3H2CF2-C8H (Micro-Epsilon Messtechnik, Germany) was used, with a temperature range from −60 °C to 200 °C. On the basis of this approach, it was determined that for the given shape and dimensions of the test sample (see Figure 2b), the heating of its surface occurred under a loading frequency 60 Hz and a stress amplitude of 610 MPa.



(**a**) (**b**)

Figure 2. Dimensions (**a**) and 3D illustration (**b**) of the est sample in accordance with standard EN 3987.

Fatigue testing of the base material was first performed at stress amplitudes (levels) as follows: 610, 580, 565, 550, 535, 520, 505, 490, 475 and 460 MPa. Subsequently, this measurement was enlarged using the "interval halving method" at stress levels of 572.5, 557.5, 542.5, 527.5, 512.5, 497.5, 482.5 and 467.5 MPa. The value of the given stress amplitude was kept constant for each stress level. As criteria for terminating of the test, we took either failure of the tested sample, or the limit of 10^7 cycles being exceeded. In total, 19 samples were tested, one for each stress amplitude, and one more on the stress amplitude 460 MPa to confirm the fatigue limit σ_C of the base material. The measured data and the final S-N curve of the base material are shown in Table 3 and Figure 3. Two basic approaches can be used to create S-N curves. The first approach requires more samples to be tested at lower stress amplitudes (levels). This approach makes it possible to determine a confidence interval for the resulting S-N curve, and was chosen, e.g., by Wu et al. [24] in their work. The second approach rests on using just one sample at higher levels of stress. The advantage of this approach is that there is more complex coverage in the area of limited life, thus resulting in its more precise definition. This second approach was chosen in this article.

Table 3. Cycles to failure N_f vs. stress amplitude σ_A of the base material—steel S700MC.

σ_A (MPa)	610	580	572.5	565	557.5	550	542.5	535	527.5	520
N_f (1)	14,618	89,479	203,831	292,247	253,012	409,694	607,374	1,011,570	1,938,660	1,680,770
σ_A (MPa)	**512.5**	**505**	**497.5**	**490**	**482.5**	**475**	**467.5**	**460**	**460**	**-**
N_f (1)	3,382,470	4,981,640	5,112,390	6,834,210	6,149,530	8,881,580	7,209,650	1.03×10^7	1.49×10^7	-

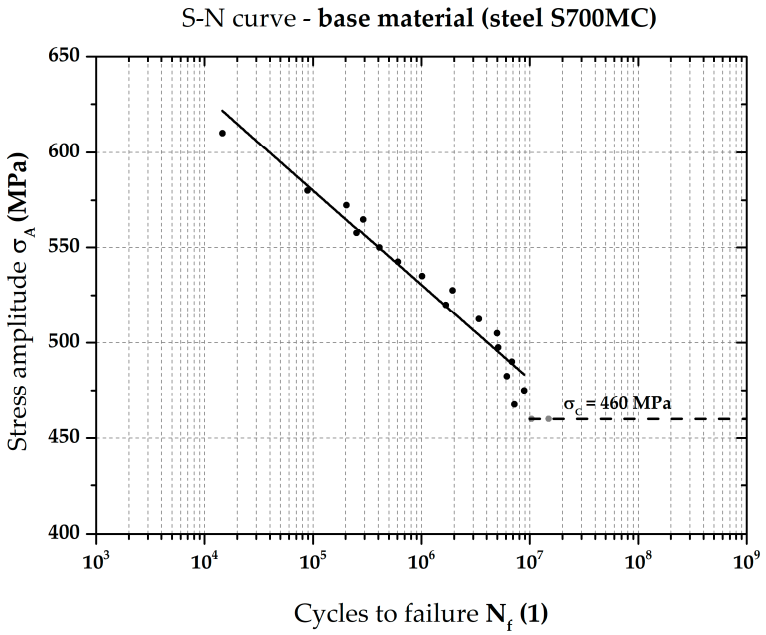


Figure 3. S-N curve (semi-log scale) of the base material—steel S700MC.

3. Welding of Testing Samples

Double-sided fillet welds were designed for fatigue testing. These were assembled from the semi-finished products with dimensions of 300 mm × 180 mm × 12 mm for the flange and 300 mm × 110 mm × 12 mm for the web. To ensure uniform contact between the web and the flange, it was necessary to machine (more precisely to mill) the web in the contact areas with the flange. Web and flange were connected to each other by two tack welds placed on the face of the weldment so that there was no influence of the fillet weld. Subsequently, the semi-automatic MAG welding method was used in the PA—flat position. The sample was not clamped in any way, so it was able to dilatate freely. As a filler material, Boehler UNION NiMoCr (BÖHLER Welding Group GmbH, Düsseldorf, Germany) was used, with a diameter of 1.2 mm and shielding gas M21 (ISO 14175). The chemical composition of the filler material (wire) is given in Table 4. Weld metal has the following material characteristics at welding with shielding gas M21: proof yield strength $R_{p0.2}$ p0.2 = 700 MPa, ultimate tensile strength Rm = 780 MPa, and impact energy KV = 100 J at RT (Room Temperature) and 47 J at −60 °C. The flow rate of the shielding gas was 15 L·min^{-1}, and the angle between torch and flange was 30°. The welding parameters were set based on previous experiments so that the heat input value reached 10.5 kJ·cm^{-1}. Welding was carried out in the synergic mode with the current value set as I = 335 A and a welding speed of 0.6 m·min^{-1}. For welding, a Migatronic BDH 550 Puls Syn (Migatronic Welding Equipment LTD, Loughborough, England) ower supply was used, and the distance between the contact die and the welding area was 15 mm. In total, three welds were prepared, all under identical conditions. Welding parameters were monitored by the WeldMonitor system (DIGITAL ELECTRIC, Brno, Czech Republic) at a scanning frequency of 20 kHz. Table 5 shows the effective measured values of voltage, current and welding speed for all weld beads. The heat input value Q (Table 5) was defined by the standard EN 1011-1. It was calculated as the product of the effective voltage and current divided by the welding speed.

Table 4. Chemical composition of filler wire Böhler UNION NiMoCrø1 (wt%).

Element	C	Si	Mn	Cr	Mo	Ni
Content (wt%)	0.08	0.60	1.70	0.20	0.50	1.50

Table 5. Actual welding process parameters measured by the WeldMonitor system.

Weld Designation	Number of Bead	Effective Current I (A)	Effective Voltage U (V)	Real Welding Speed v_s (m·min^{-1})	Heat Input Q (J·mm^{-1})
Weld 1	1	353.2	29.7	0.601	**1.047**
	2	348.6	29.8	0.599	**1.041**
Weld 2	1	351.7	29.7	0.597	**1.050**
	2	347.9	29.8	0.599	**1.039**
Weld 3	1	354.3	29.8	0.602	**1.052**
	2	350.5	29.7	0.600	**1.041**

Generally, due to the dilation of welds, there is a deformation of the web and the flange. However, in this case, welds were only stressed in the flange direction, and thus the subsequent measurement of angular deformation after passing the 1st and 2nd bead was performed in the way shown in Figure 4. From the beginning of the weld, 13 points were taken in this direction at which the angular deformation was measured; thus, the distance between the individual measuring points was 25 mm (see 1st column in Table 6).

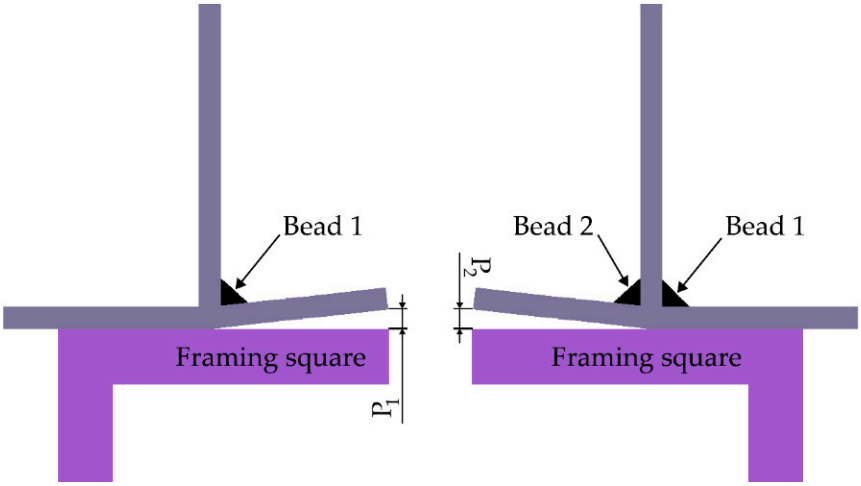


Figure 4. Measurement of angular deformation after welding.

Table 6. Measured values of angular deformation (in accordance with Figure 4).

Distance (mm)	Weld 1		Weld 2		Weld 3	
	P1 (mm)	P2 (mm)	P1 (mm)	P2 (mm)	P1 (mm)	P2 (mm)
0	1.60	3.03	1.67	3.16	1.59	3.11
25	1.63	3.11	1.58	2.99	1.55	3.09
50	1.67	3.18	1.59	3.00	1.58	3.25
75	1.71	3.16	1.65	3.17	1.69	3.28
100	1.78	3.19	1.71	3.29	1.73	3.24
125	1.77	3.21	1.79	3.21	1.74	3.26
150	1.72	3.13	1.75	3.12	1.66	3.17
175	1.73	3.07	1.70	3.08	1.68	3.09
200	1.69	2.99	1.64	3.16	1.62	3.01
225	1.68	2.96	1.65	3.08	1.63	3.03
250	1.65	2.94	1.61	3.04	1.59	2.98
275	1.61	2.94	1.63	2.99	1.57	2.96
300	1.58	2.91	1,66	3.02	1.62	2.95
Average Value	**1.68 ± 0.06**	**3.06 ± 0.11**	**1.66 ± 0.06**	**3.10 ± 0.09**	**1.63 ± 0.06**	**3.09 ± 0.12**

In Table 6, the measured values of angular deformation after welding the first and second weld bead are shown for all three welds. The difference between the average values of angular deformation in all three welds was lower than 3%—after both the first and second bead. The standard deviation of deformation of the sample did not exceed 4%.

For every welded sample, the beginning and end length of the weld was cut off at a distance of 35 mm, that is, in the area where the temperature field is already stable. Right in this area, a metallographic scratch pattern of the weld and a geometrical evaluation of both beads were performed. The differences in the geometrical evaluation among the individual welds were very small, and differences between the individual measured quantities didn't exceed 4%. However, only in the case of Weld 2, the difference in the penetration depth was equal to 9%. Therefore, the geometrical evaluation only for Weld 2 is shown in Figure 5.

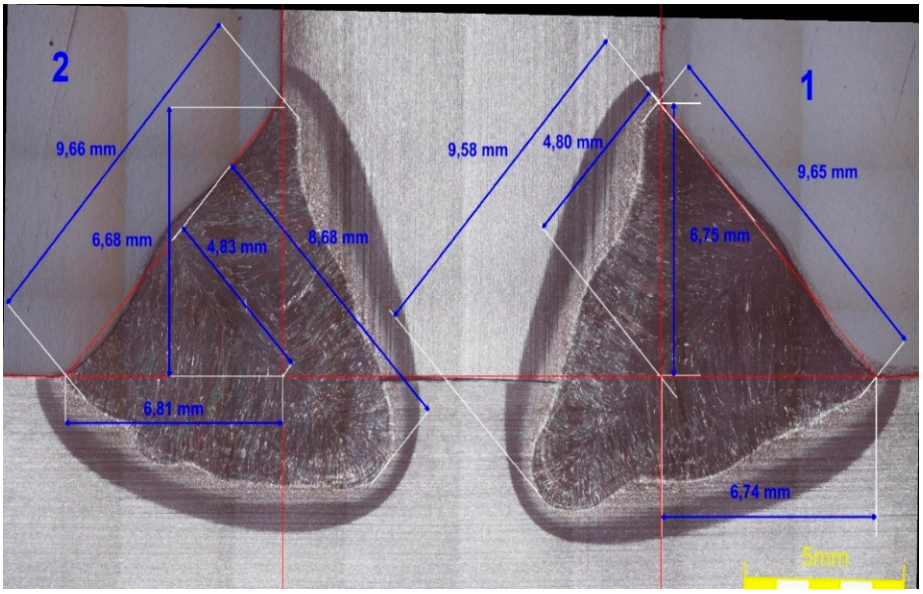


Figure 5. Geometrical evaluation of Weld 2 after welding of the tested material—steel S700MC (etched by 3% Nital).

To assess the effect of the welding process on changes in HAZ, Vickers hardness measurements and measurements of grain coarsening were performed in a highly heated HAZ. The hardness measurement HV 5 (in accordance with the standard EN ISO 6507-1) was performed from the base material across the HAZ, to the weld metal, again across HAZ and back to the base material. The distance between the individual indentations was 1.0 mm in the weld metal and 0.5 mm in the base material and the HAZ. As can be seen from Figure 6, below (Weld 1 and Bead 1), the highest hardness values were measured to be about 0.5 mm from the fusion line. However, due to the very low carbon content, the hardness in the HAZ increased by less than 40 HV 5 compared to the base material.

Grain coarsening analysis in the HAZ was performed using a Tescan MIRA electron microscope (Tescan Orsay holding a.s., Brno, Czech Republic) using EBSD analysis at the location of Bead 1 on Weld 1. At first, an area with a width of 0.4 mm and a length of 2.5 mm at the transition from weld metal to HAZ was scanned. The details of this transition from the highly heated area to the normalization area in the HAZ are shown in Figure 7. Furthermore, the grain size in the highly heated area of the HAZ was measured by EBSD analysis from the fusion line to a distance of 0.3 mm. This measurement was performed along the fusion line in three areas with a size of 0.3 mm $\times$ 0.4 mm and the three average values of grain size (d_1 = 13.06 µm, d_2 = 12.87 µm and d_3 = 13.14 µm) were obtained. Therefore, the average grain size in a highly heated HAZ was $d_{HAZ} = 13.02 \pm 0.14$ µm.

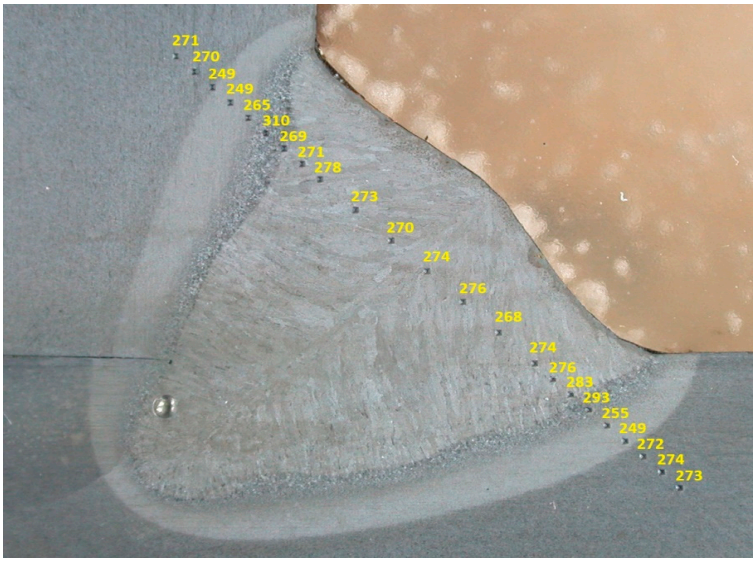


Figure 6. HV5 hardness measurement after the welding of HSLA steel S700MC (Weld 1, Bead 1).

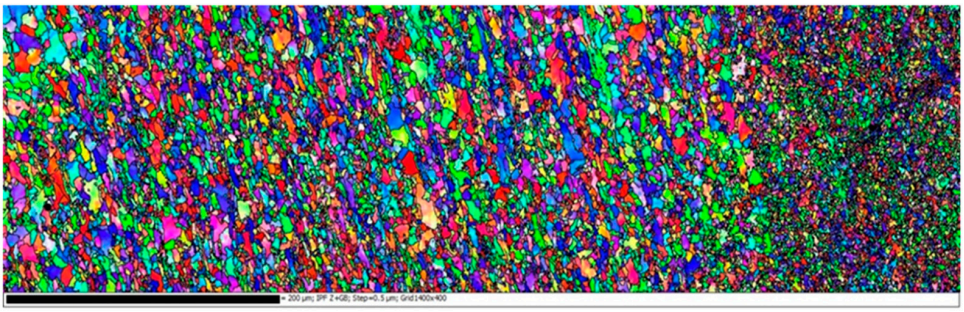
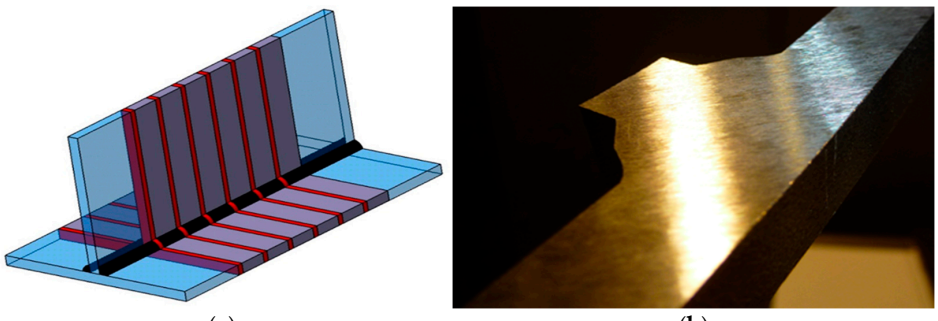


Figure 7. Details of grain coarsening in the HAZ after welding of steel S700MC (Weld 1, Bead 1).

4. Preparation of Samples for Fatigue Testing

As already mentioned in Section 3, the initial and final 35 mm of the weld length was cut off for all welded joints so that the samples used for the subsequent fatigue tests were taken right from the stable temperature field. After that, for the fatigue testing, 11 testing samples with a width of 18 mm were prepared from every weld cut, as schematically shown in Figure 8a. Cyclic loading was planned to be in the flange direction, so the web was removed from the weld at a distance 15 mm for every sample. In addition, surface grinding was also used on the edges of the test samples to reduce the influence of the notch effect after cutting. Moreover, this machining operation was performed under intense cooling to reduce the thermal effect as much as possible. The prepared test sample for the subsequent fatigue testing is shown in Figure 8b.



(**a**) (**b**)

Figure 8. Cyclic testing: (**a**) cutting of test samples; (**b**) completely prepared test sample.

5. Fatigue Life Determination of the Welded Samples

First, the samples prepared as described in Chapter 4 were tested by cyclic loading. Although the difference between the average values of angular deformation for all three welds was lower than 3% and the standard deviation of deformation did not exceed 4%, it was decided to select 10 samples with the same deformation for the first test series. Therefore, the maximum differences in angular deformations for the first 10 samples were lower than 1.5%. All welds were loaded in the flange direction, as schematically shown in Figure 9; the testing length of welded sample between the grips was 50 mm. A servo-hydraulic testing device INOVA FU-O-1600-V2 (INOVA GmbH, Bad Schwalbach, Germany), was used again for fatigue testing in the controlled force mode. The samples were loaded using a fully reversed harmonic cycle (purely alternating stress) with the stress ratio (cycle asymmetry) R = -1 under the following stress amplitudes (levels): 420, 370, 320, 270, 220, 170, 120, 110, 105 and 100 MPa. These stress amplitudes were chosen based on the preliminarily performed experiments. The loading frequency was lowered by 20 Hz compared to the base material, due to the larger cross-section area of the sample, and thus also to the higher force amplitudes. The same test termination criteria were also used in this kind of fatigue test, i.e., fatigue crack initialization or achieving the fatigue limit of 10^7 cycles.

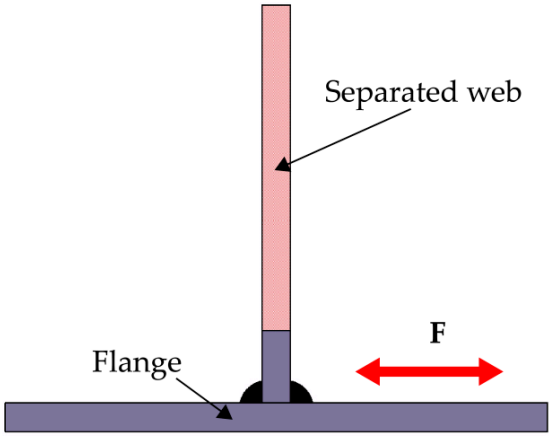


Figure 9. Shape adjustment and loading of fatigue tests.

Table 7 summarizes the results of the fatigue tests for all of the tested basic welds. The measured S-N curve of the basic welded samples of the material S700MC is given in Figure 10. On the basis of these results, the fatigue limit of the basic welded samples from material S700MC was determined to be σ_C = 100 MPa. Subsequently, one more test of the welded sample was performed at a stress level of 100 MPa to confirm the determined value of fatigue limit σc. In this way, crucial basic information was obtained about welded joint fatigue life with the cumulative influence of all monitored aspects of the welding process (i.e., influence of angular deformation, notch effect of the weld bead and changes in the HAZ of weld). The fatigue failure of all samples was observed at stress amplitudes from 420 MPa to 105 MPa right at the interface between the flange and the weld bead.

Table 7. Cycles to failure N_f vs. stress amplitude σ_A of basic welded samples—steel S700MC.

σ_A (MPa)	420	370	320	270	220	170	120	110	105	100	100
N_f (1)	7257	11,498	24,089	49,563	64,277	231,763	766,911	1,804,877	3,026,921	10^7	10^7

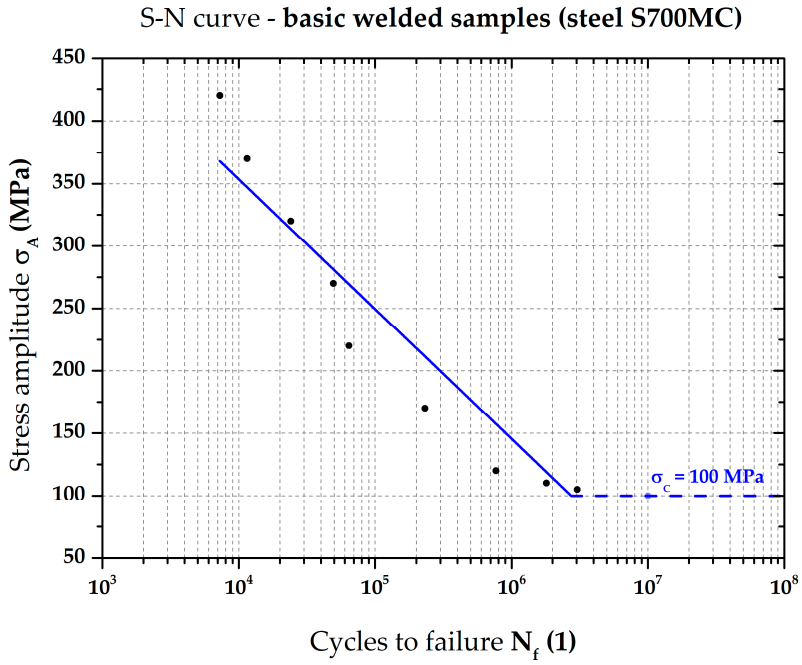


Figure 10. S-N curve (semi-log scale) of basic welded samples—steel S700MC.

5.1. Fatigue Life Determination of Welded Samples without the Influence of Angular Deformation

To quantify the influence of angular deformation after welding on the change of fatigue life, it was necessary to adjust the testing samples in order to restrain the effect of angular deformation. This modification of the samples was done by milling. At first, sample was aligned in the bench vice using a dial indicator so that both deformed flange arms were at the same height. Simultaneously, the flatness of areas at the transition from the base material to the weld bead was checked. After alignment, the two deformed parts of the flange were milled so that the machined surface passed smoothly into the original surface at a distance of 1.5 to 2 mm from the transition area between the base material and the weld bead. After that, the sample was rotated, aligned on the machined surfaces, and the whole lower edge of flange was milled to a plane to reveal as little flange thinning as possible. As a result, a total of 11 samples were obtained, all of them with zero angular deformation. This production method of modifying test samples is schematically shown in Figure 11. The milled areas of deformed flange are shown in red.

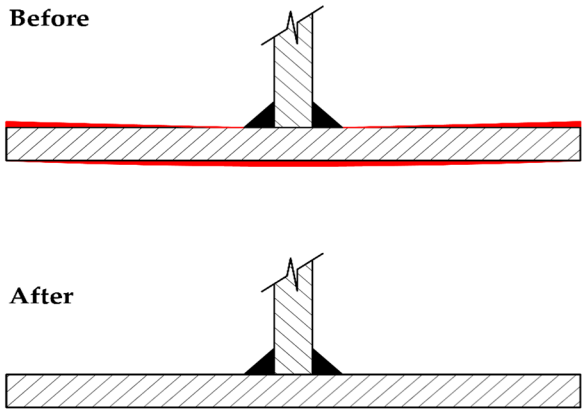


Figure 11. Schematic representation of the test sample flange modification.

As in the case of original unmodified samples, these specimens were also stressed with a fully reversed harmonic cycle (purely alternating stress) with the stress ratio R = −1. The loading frequency in this case was 20 Hz. Testing started on the same six stress amplitudes

as before, so at 420, 370, 320, 270, 220, 170 MPa. In addition to that, the following stress amplitudes were applied: 470, 150, 140 and 130 MPa. The criterion for terminating the test also remained the same. The last, eleventh, sample was used to confirm the measured magnitude of fatigue limit σc at the stress level of 130 MPa. The measured data are given in Table 8, and a graphical illustration of fatigue behaviour is shown in Figure 12 via the S-N curve of the welded samples without the influence of angular deformation. Moreover, in this case (samples without influence of angular deformation), too, a crack was initiated at the interface between the flange and the weld bead.

Table 8. N_f vs. σ_A of welded samples without influence of angular deformation.

σ_A (MPa)	470	420	370	320	270	220	170	150	140	130	130
N_f (1)	7931	13,611	22,973	63,235	129,164	334,854	1,208,016	1,989,038	3,725,785	10^7	10^7

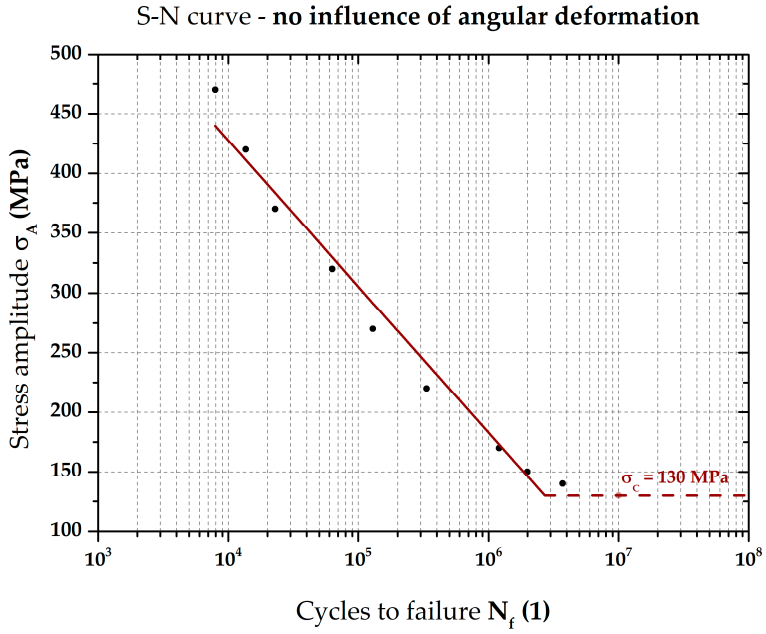


Figure 12. S-N curve (semi-log scale) of the welded samples without the influence of angular deformation.

5.2. Fatigue Life of Samples without the Influence of Angular Deformation and Notch Effect

To assess the effect of changes that occur in the HAZ of welds, samples had to be modified not only to eliminate angular deformation, but also to restrain the notch effect caused by the weld geometry. Therefore, all remaining samples were first milled as described in Section 5.1 to eliminate the influence of deformation after welding. Subsequently, it was necessary to adjust the welds so as to eliminate the notch effect of the weld bead, while maintaining the influence of HAZ. Due to the evaluated weld geometry (Figure 5), it was possible to propose an optimal radius, which revealed a tangential direction both to the transition from flange to weld and to the transition from weld to web. For all six prepared weld beads (on three welds), this radius was as follows: R = 5.73 ± 0.11 mm. However, it is quite difficult to produce such individual radii. On the other hand, due to the loading type of samples that are in the flange direction, it is sufficient to eliminate the notch effect only at the transition from flange to weld. Such modification can be performed using commonly supplied tools with radius R = 6 mm. Thus, all remaining test samples were modified in this way. The method of preparation of these test samples is shown in the schematic in Figure 13a, where the milled areas of the deformed flange (as well as the radius milled into the weld) are again shown in red. Figure 13b shows a sample that has already been prepared for fatigue testing.

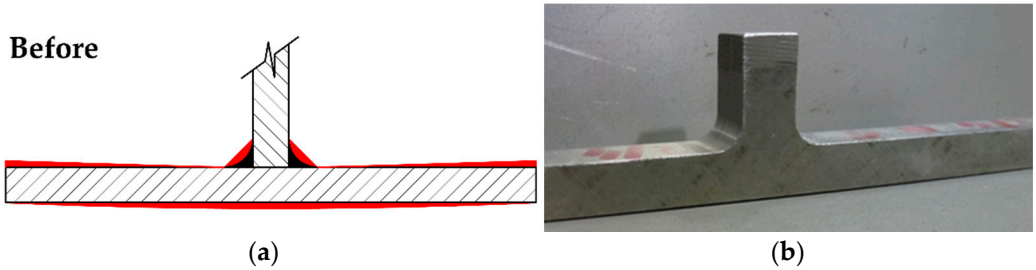


Figure 13. Schematic representation of modifications: (**a**) flange and weld bead; (**b**) real sample.

Our own testing method of fatigue loading was again performed in the same way as in the previous experiment. Thus, a fully reversed harmonic cycle (purely alternating stress) with the stress ratio R = −1 was again used. The loading frequency was 20 Hz. Testing started at the following five stress amplitudes: 470, 420, 370, 320 and 270 MPa. These stress amplitudes were subsequently added by measurements at 570, 520, 270, 260 and 250 MPa. Additionally, the criteria for terminating the test remained the same: failure of the tested sample or achieving a fatigue limit of 10^7 cycles. In seven of the nine total tested samples, a crack was initiated in the area corresponding to HAZ in the flange. The sample that was loaded at a stress level of 520 MPa had a crack in the flange at a distance of about 4 mm from the HAZ, and the sample loaded at stress level of 270 MPa had a crack in the flange at a distance of ca. 10 mm from the HAZ, but after 3×10^6 cycles (in Figure 14, this result is shown in red and wasn't included in the data for the construction of the S-N curve). The measurement of the stress amplitude 270 MPa was repeated, and a new sample revealed a fracture in the flange HAZ after 2,830,010 cycles. The first and second verification samples at a stress level of 250 MPa achieved cycles to failure of more than 1.1×10^7 and 1.05×10^7, both without failure. The data from this part of the fatigue testing (welded samples without any influence) are shown in Table 9. The obtained S-N curve of these welded samples without influence of angular deformation as well as notch effect is shown in Figure 14.

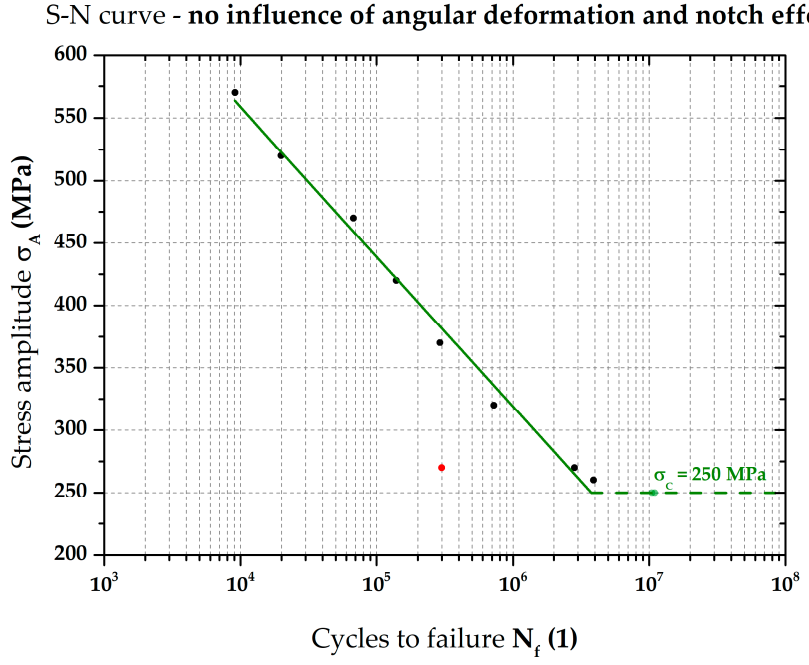


Figure 14. S-N curve (semi-log scale) of welded samples without the influence of angular deformation and notch effect.

Table 9. N_f vs. σ_A of welded samples without the influence of angular deformation.

σ_A (MPa)	570	520	470	420	370	320	270	260	250	250
N_f (1)	9113	19,839	67,511	139,254	291,378	723,172	2,830,010	3,901,817	1.1×10^7	1.05×10^7

6. Discussion

Fatigue life in the area of limited life (termed as the fatigue strength σ_N) and also the fatigue (endurance) limit σ_C are absolutely essential material characteristics for all dynamically stressed parts. Such information is especially necessary in the automotive industry and, e.g., in the still increasing application of HSLA steels. Obtaining the S-N curves of the base materials is quite easy. However, it is already much more difficult with welded joints. The welding process results in there being a lot of aspects influencing fatigue life. Moreover, they have different effects. Therefore, it is very difficult to assess which aspects are more important from a design and technological point of view.

Several authors [18–22] have studied the problem of fatigue behaviour of HSLA steel welded joints. Works published in this area differ from each other mainly with respect to the type of steel used, the type of stressed joint, the loading method and in light of the welding technology used. However, all papers evaluate the final weld as a whole, without the possibility of quantifying the individual aspects of own welding process. Nevertheless, it is very difficult to optimize the whole welding process without these partial data. Thus, the major contribution of this paper rests in description of these partial aspects of the whole process and to try, for one of the most used HSLA steels (to be more specific S700MC), to determine the importance of such influences.

Thus, in this paper, the influence of angular deformation and the notch effect of the weld, as well as influence of changes that occur in HAZ of welds was evaluated. As described in Chapter 5, the influence of individual aspects could be gradually eliminated through the geometrical modification of welded samples. From the comparison the individual S-N curves (Figures 10, 12 and 14) could be used to determine the importance (or more precisely degree of influence) of the partial aspects influencing the welding process. The complete comparison, including all testing conditions (base material, basic samples, samples without influence of angular deformation, and samples without influence both of angular deformation and notch effect), is shown in Figure 15. As already mentioned in Section 2, the S-N curves were plotted by using individual measurements at greater stress levels. The reason was the necessity of comparing individual influences of the welding process.

From Figure 15, it is evident that the welding process (blue S-N curve) significantly reduced the value of steel S700MC fatigue limit σ_C. This fatigue limit was reduced by 360 MPa to 100 MPa, which is more than 78%. There is also a significant difference in the slope of the relevant line in the area of limited life, which is much flatter for the base material. The reasons for such significant changes in fatigue strength arise mainly from the notch effect of the weld, material changes in HAZ and additional bending stresses caused by deformation after welding. However, the size and shape factor of the test samples used also has a partial influence. To assess these partial effects, it was necessary to compare the individual S-N curves of welded joints.

The effect of angular deformation can be determined by mutual comparison of the S-N curves illustrating the fatigue behaviour of the test samples without the influence of angular deformations (Figure 15—red line) and S-N curve of basic samples (just as they were welded); see Figure 15 (blue line). The fatigue limit σ_C for samples without the effect of angular deformation increased by 30 MPa to 130 MPa. From these results, it can be concluded that the bending stresses contribute to the reduction base material fatigue limit by approximately 6%, and to the overall influence of welding process by 8.3%. However, this is only valid for the used loading method and clamping of samples on the fatigue testing device, when the distance between the testing grips was 50 mm. If the distance between clamping grips is increased, the magnitude of the bending moment

would increase, and thus also the effect of combined bending stress would also slightly increase. However, this effect would probably not exceed 10%.

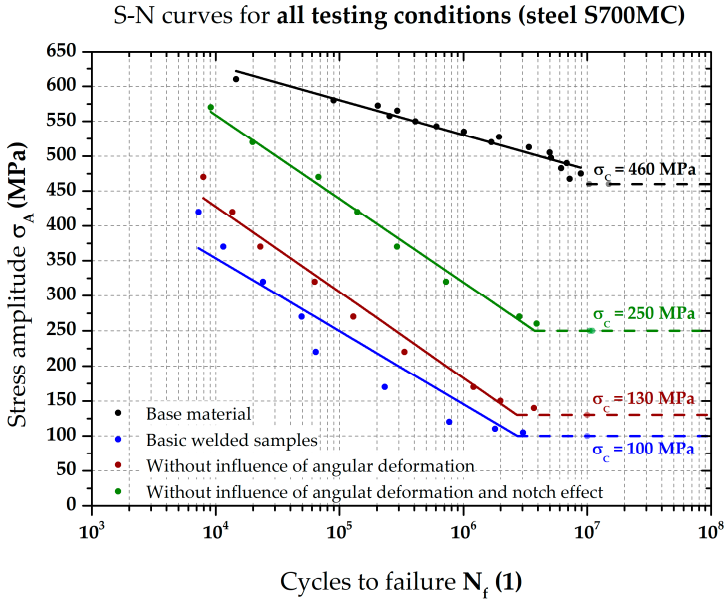


Figure 15. Comparison of the final S-N curves (semi-log scale) regarding observed aspects of welding process.

The influence of the notch effect caused due to the weld bead geometry could be assessed by the notch elimination, i.e., by a smooth transition from flange to web. Because of this, samples without the influence of angular deformation and with a radius R6 on transition from the flange to the web were used. The fatigue limit σ_C = 250 MPa was measured by fatigue testing (Figure 15—olive line), which means an increase of fatigue limit already by 150 MPa, compared to the basic welded samples. Thus, after deduction the effect of angular deformation, notch effect of weld contributed to the base material fatigue limit reduction by 26.6%. Finally, its share in the total welding process influence was 33.4%.

By means of a simple sum, it can be determined that the angular deformation after welding and the notch effect given by the welding bead geometry contribute to the fatigue limit reduction caused by welding approximately by 42%. The rest, i.e., about 58% of such effect, deals with the changes that occur in HAZ due to welding. However, this claim cannot be fully accepted, because the size and the shape factor of the testing samples used need to also be taken into account. This approach would be possible to use under the condition that samples defined by standard EN 3987 would not be used when measuring the S-N curve of the base material (see Figure 2), but rather modified samples corresponding in shape and dimensions to the testing samples used. These samples would have a rectangular cross-section area with a width of 18 mm and a height of at least 8 mm. Then it would be possible to precisely determine the effect of the changes that occur during welding in the HAZ of welds. Therefore, further work by the authors' team in this area will be focused on assessing the influence of size and shape factor in HSLA steels.

It was not possible to compare the obtained results with similar works, because it was not possible to find any published scientific studies devoted to the quantification of the influence of partial aspects of the welding process on changes in fatigue behaviour (fatigue limit).

7. Conclusions

The main aim of the presented paper was to assess and quantify the influence of partial aspects of the welding process on the fatigue limit of fillet welds from HSLA steel S700MC. The work managed to create a methodology for the preparation of testing samples

so that it is possible to quantify selected partial aspects of the welding process. However, as is clear from the discussion of the results, the need to focus research also on other branches, as well as to take into account other aspects (e.g., influence of size and shape factor), also became apparent. Moreover, it wasn't possible to compare the results with other works, as similar findings have not yet been published for HSLA steels. The experimentally obtained knowledge in this work can be summarized in the following points:

(1) The process of welding double-sided fillet welds using the MAG welding method significantly reduced the fatigue limit of steel S700MC, despite the fact that the heat input value was limited to Q = 10 kJ·cm^{-1}, as is required for the fine-grained steels of higher strengths. The magnitude of the fatigue limit σ_C decreased from 460 MPa to 100 MPa, i.e., by 78%.

(2) Although the angular deformation occurring during welding has an effect on the change of fatigue life, this effect isn't as significant as in the case of other aspects. For the given loading conditions, angular deformation contributed to reductions in the base material fatigue limit by 6% and to the overall influence of welding process by 8.3%.

(3) The notch effect caused by the weld bead geometry has a much greater effect. For the given welding conditions, this aspect contributed to reductions in the base material fatigue limit by 26% and to the overall influence of welding process by 33%.

(4) Changes occurring during welding of HSLA steels in HAZ had the greatest effect on reduction the fatigue limit σ_C of steel S700MC. However, it should be added that this is a superposition of influence that includes the effect of welding and size and the shape factor of the used testing samples.

It can be assumed that with lower heat input values, there will be a higher influence of the fillet weld notch effect. Lower values of current I, as well as lower heat input values Q, will cause changes in welding bead geometry. Thus, the excess weld metal will increase, and simultaneously also the notch effect. On the other hand, when the heat input value Q is reduced, there won't be such large changes in the HAZ, and thus there will also be a lower impact on the fatigue limit.

When assessing the influence of partial welding aspects on fatigue life, the authors recommend using samples with a cross-section area similar in shape and dimensions to those planned for testing welded joints when creating the resulting S-N diagrams.

Author Contributions: Conceptualization, J.M.; methodology, J.M. and I.N.; investigation, J.M., J.S., I.N. and S.B.; resources, J.M., I.N. and S.B.; data curation, J.M. and J.S.; writing—original draft preparation, J.M., writing—review and editing, J.M. and J.S.; visualization, J.M. and J.S. All authors have read and agreed to the published version of the manuscript.

Funding: This research was funded by the Student Grant Competition of the Technical University of Liberec under the project No. SGS-2019-5015 "Research and development for innovation of materials and production technologies with application potential in mechanical engineering".

Institutional Review Board Statement: Not applicable.

Informed Consent Statement: Not applicable.

Data Availability Statement: Not applicable.

Conflicts of Interest: The authors declare no conflict of interest.

References

1. Illescas, S.; Fernández, J.; Asensio, J.; Sánchez-Soto, M.; Guilemany, J.M. Study of the Mechanical Properties of Low Carbon Content HSLA Steels. *Rev. Metal.* **2009**, *45*, 424–431. [CrossRef]
2. Moravec, J.; Novakova, I.; Sobotka, J.; Neumann, H. Determination of Grain Growth Kinetics and Assessment of Welding Effect on Properties of S700MC Steel in the HAZ of Welded Joints. *Metals* **2019**, *9*, 707. [CrossRef]
3. Pamnani, R.; Jayakumar, T.; Vasudevan, M.; Sakthivel, T. Investigations on the Impact Toughness of HSLA Steel Arc Welded Joints. *J. Manuf. Process.* **2016**, *21*, 75–86. [CrossRef]

4. Sastry, C.C.; Hariharan, P.; Kumar, M.P.; Manickam, M.A.M. Experimental Investigation on Boring of HSLA ASTM A36 Steel under Dry, Wet, and Cryogenic Environments. *Mater. Manuf. Process.* **2019**, *34*, 1352–1379. [CrossRef]
5. Barbaro, F.; Kuzmikova, L.; Zhu, Z.; Li, H. Weld Haz Properties in Modern High Strength Niobium Pipeline Steels. In Proceedings of the Energy Materials 2014; Springer International Publishing: Cham, Germany, 2016; pp. 657–664.
6. Fernández, J.; Illescas, S.; Guilemany, J.M. Effect of Microalloying Elements on the Austenitic Grain Growth in a Low Carbon HSLA Steel. *Mater. Lett.* **2007**, *61*, 2389–2392. [CrossRef]
7. Schaupp, T.; Schroepfer, D.; Kromm, A.; Kannengiesser, T. Welding Residual Stresses in 960MPa Grade QT and TMCP High-Strength Steels. *J. Manuf. Process.* **2017**, *27*, 226–232. [CrossRef]
8. Branco, R.; Berto, F. Mechanical Behavior of High-Strength, Low-Alloy Steels. *Metals* **2018**, *8*, 610. [CrossRef]
9. Laitila, J.; Larkiola, J. Effect of Enhanced Cooling on Mechanical Properties of a Multipass Welded Martensitic Steel. *Weld World* **2019**, *63*, 637–646. [CrossRef]
10. Njock Bayock, F.; Kah, P.; Mvola, B.; Layus, P. Effect of Heat Input and Undermatched Filler Wire on the Microstructure and Mechanical Properties of Dissimilar S700MC/S960QC High-Strength Steels. *Metals* **2019**, *9*, 883. [CrossRef]
11. Taavitsainen, J.; da Silva, P.S.V.; Porter, D.; Suikkanen, P. Weldability of Direct-Quenched Steel with a Yield Stress of 960 MPa. In Proceedings of the 10th International Conference on Trends in Welding Research and 9th International Welding Symposium of Japan Welding Society (9WS), Tokyo, Japan, 11–14 October 2016; Curran Associates, Inc.: New York, NY, USA, 2017; pp. 52–55.
12. Górka, J. Microstructure and Properties of the High-Temperature (HAZ) of Thermo-Mechanically Treated S700MC High-Yield-Strength Steel. *Mater. Tehnol.* **2016**, *50*, 616–621. [CrossRef]
13. Skowrónska, B.; Chmielewski, T.; Golański, D.; Szulc, J. Weldability of S700MC Steel Welded with the Hybrid Plasma+ MAG Method. *Manuf. Rev.* **2020**, *7*, 4. [CrossRef]
14. Mičian, M.; Harmaniak, D.; Nový, F.; Winczek, J.; Moravec, J.; Trško, L. Effect of the T8/5 Cooling Time on the Properties of S960MC Steel in the HAZ of Welded Joints Evaluated by Thermal Physical Simulation. *Metals* **2020**, *10*, 229. [CrossRef]
15. Fydrych, D.; Tomków, J.; Rogalski, G.; Labanowski, J. Weldability of S460ML High Strength Low Alloy Steel in Underwater Conditions. *Appl. Mech. Mater.* **2016**, *838*, 10–17. [CrossRef]
16. Kik, T.; Górka, J.; Kotarska, A.; Poloczek, T. Numerical Verification of Tests on the Influence of the Imposed Thermal Cycles on the Structure and Properties of the S700MC Heat-Affected Zone. *Metals* **2020**, *10*, 974. [CrossRef]
17. Kik, T.; Moravec, J.; Švec, M. Experiments and Numerical Simulations of the Annealing Temperature Influence on the Residual Stresses Level in S700MC Steel Welded Elements. *Materials* **2020**, *13*, 5289. [CrossRef]
18. Šebestová, H.; Horník, P.; Mrňa, L.; Jambor, M.; Horník, V.; Pokorný, P.; Hutař, P.; Ambrož, O.; Doležal, P. Fatigue Properties of Laser and Hybrid Laser-TIG Welds of Thermo-Mechanically Rolled Steels. *Mater. Sci. Eng. A* **2020**, *772*, 138780. [CrossRef]
19. Moravec, J.; Sobotka, J.; Solfronk, P.; Thakral, R. Heat Input Influence on the Fatigue Life of Welds from Steel S460MC. *Metals* **2020**, *10*, 1288. [CrossRef]
20. Lahtinen, T.; Vilaça, P.; Infante, V. Fatigue Behavior of MAG Welds of Thermo-Mechanically Processed 700MC Ultra High Strength Steel. *Int. J. Fatigue* **2019**, *126*, 62–71. [CrossRef]
21. Lago, J.; Trško, L.; Jambor, M.; Nový, F.; Bokůvka, O.; Mičian, M.; Pastorek, F. Fatigue Life Improvement of the High Strength Steel Welded Joints by Ultrasonic Impact Peening. *Metals* **2019**, *9*, 619. [CrossRef]
22. Kim, Y.; Hwang, W. Effect of Weld Seam Orientation and Welding Process on Fatigue Fracture Behaviors of HSLA Steel Weld Joints. *Int. J. Fatigue* **2020**, *137*, 105644. [CrossRef]
23. Schmidová, E.; Bozkurt, F.; Culek, B.; Kumar, S.; Kuchariková, L.; Uhríčik, M. Influence of Welding on Dynamic Fracture Toughness of Strenx 700MC Steel. *Metals* **2019**, *9*, 494. [CrossRef]
24. Wu, S.C.; Qin, Q.B.; Hu, Y.N.; Branco, R.; Li, C.H.; Williams, C.J.; Zhang, W.H. The Microstructure, Mechanical, and Fatigue Behaviours of MAG Welded G20Mn5 Cast Steel. *Fatigue Fract. Eng. Mater. Struct.* **2020**, *43*, 1051–1063. [CrossRef]